REGENERATION

The synovial environment steers cartilage deterioration and regeneration

Johanna Bolander[1,2]*, Maria Teresita Moviglia Brandolina[3], Gary Poehling[1,4], Olivia Jochl[1], Emma Parsons[1], William Vaughan[1], Gustavo Moviglia[1,3]†, Anthony Atala[1]†

Osteoarthritis (OA) was recently defined as an epidemic, and the lack of effective treatment is highly correlated to the limited knowledge regarding the underlying pathophysiology. Failure to regenerate upon trauma is thought to be one of the underlying causes for degenerative diseases, including OA. To investigate why lesions within an OA environment fail to heal, a heterogeneous cell population was isolated from the synovial fluid (SF) of OA patients. The cells' ability to undergo processes required for functional tissue regeneration was evaluated in the presence or absence of autologous SF. The obtained mechanistic findings were then used for the development of an immunomodulatory cell treatment, aimed to restore the pro-regenerative environment. Intra-articular injection in a clinical compassionate use study showed that the treatment restored the articular cartilage and joint homeostasis of OA patients. These findings confirm the role of pro-regenerative immune cells and their targeted influence on progenitor cells for degenerative joint disease therapies.

INTRODUCTION

Fibrosis is initiated by failed regeneration and, when excessive, may lead to organ malfunction. This detrimental effect makes fibrosis the main cause of more than 45% of deaths in the industrialized world today (*1*). One of the most common diseases caused by fibrosis is osteoarthritis (OA), affecting more than 520 million people worldwide (*2*). Because of its degenerative nature, OA causes severe pain, functional loss, and disability. With no cure available, treatments of OA mainly focus on managing pain and limiting disease progression. When this can no longer be controlled, joint replacement is the final option. Traumatic joint injury is a major cause of OA. The onset of the disease can be further initiated by the complexity and size of the injury, repeated injury, age, genetic prevalence, and/or lifestyle. Commonly, initial trauma fails to heal because of a prolonged pro-inflammatory response, leading to the initiation of fibrosis and the accumulation of excessive connective tissue as a result of the failed regeneration (*3*).

In a healthy regenerative environment, the general tissue response to trauma includes an immediate activation of pro-inflammatory neutrophils, leading to decontamination and clearing of debris at the injury site and recruitment of infiltrating monocytes. Next, neutrophil-secreted cytokines steer differentiation of activated monocytes into macrophages, which remove apoptotic cells and function as antigen-presenting cells for the anti-inflammatory and pro-regenerative helper T cells (T cells) specifically activated for the injured tissue (*4*). This step prevents further leukocyte influx and steers the injured environment toward a pro-regenerative process. The successful initiation of the pro-regenerative phase leads to the recruitment of progenitor cells that, under guidance by the pro-regenerative immune cells, contribute to tissue regeneration (*5*). Consequently, the signaling cascades that steer the balance, polarization, and subsequent action of the immune cells, including T helper 1 (T_H1), T_H2, and T_H17 and T regulatory cells, macrophages, and mast cells, are crucial for functional transition to the pro-regenerative phase (*6*, *7*). During the initiation of OA, the pro-inflammatory response persists as evidenced by (i) pro-inflammatory cells in the synovial fluid (SF), (ii) pro-inflammatory cytokines in the SF, and (iii) articular cartilage deterioration (*8*).

Full-thickness osteochondral microdefects in juvenile mice have shown the potential to heal. Healing is preceded by a thickening of the synovial membrane 7 days after injury, in combination with proliferating $CD44^+$ and Proteoglycan 4 ($PRG4^+$) progenitor cells that later fill the defect environment (*9*). On the basis of these findings, it can be hypothesized that functional regeneration of osteochondral defects may occur through the activation of appropriate progenitor cells recruited from the surrounding tissues, such as the synovial membrane, upon the onset of the pro-regenerative phase from the local immune cells. Once these progenitors are activated by trauma, they migrate to the defect site where they attach, proliferate, and undergo chondrogenic differentiation to contribute to tissue regeneration. Subsequently, it can be hypothesized that elements in the synovial OA environment may interfere with any of these crucial steps, impairing the regenerative potential. These elements would then be a cause, and as a result, a target to treat and potentially cure OA in a clinically effective way. The SF from OA patients was herein identified to be a major inhibitor of the regenerative process in an OA environment. Specifically, the heterogeneous cell population isolated from the SF showed a clear ability to migrate, attach, proliferate, and undergo chondrogenic differentiation, all steps crucial for functional regeneration to occur, under standard assay conditions. However, the presence of autologous SF (aSF) during any of these events drastically impaired these processes. Characterization of the SF cytokine composition linked these results to a specific pro-inflammatory profile, suggesting an imbalance between pro- and anti-inflammatory immune cells in the SF. On the basis of these findings, an immunomodulatory cell treatment was developed with the goal of restoring joint homeostasis

[1]Wake Forest Institute for Regenerative Medicine, Wake Forest School of Medicine, Winston Salem, NC, USA. [2]Skeletal Biology and Research Engineering Center, KU Leuven, Leuven, Belgium. [3]Civil Association of Research and Development of Advanced Therapies (ACIDTA), CABA, Argentina. [4]Department of Orthopaedic Surgery, Wake Forest Baptist Health, Winston Salem, NC, USA.
*Corresponding author: jbolande@wakehealth.edu
†These authors contributed equally to this work.

by mimicking crucial events seen during tissue regeneration. The treatment was based on anti-inflammatory cartilage-activated T cells (CATs), which upon coculture with adipose-derived mesenchymal stromal cells (aMSCs), induced chondrogenic priming of the progenitor cells. Intra-articular injection of the final coculture steered articular cartilage regeneration and restored joint homeostasis in a rat OA model. Clinical evaluation showed improved quality of life, reduced pain, and articular cartilage regeneration in a compassionate use study.

RESULTS

SF-derived cells of OA patients can undergo processes required for functional regeneration

To evaluate SF-derived cells′ ability to contribute to the regenerative process upon trauma, SF was collected from OA patients during appointments for joint pain and swelling. The cellular and fluid portions were separated, and in vitro expanded cells were labeled, resuspended in growth medium (GM), and seeded in a migration chamber. To evaluate the cells′ ability to migrate in response to injury, chondrocyte lysate (CL) was used as an attractant, with or without the presence of 10% aSF (CL/SF). It was found that the cells migrated to a similar extent with CL alone or with the addition of SF as an attractant (Fig. 1A). However, when SF was added to the GM, without impairing the viscosity of the media, cell migration was drastically impaired, independent of attractant (Fig. 1A). Next, the SF-derived cells′ ability to attach to the tissue culture surface was investigated by morphological observation through bright-field microscopy 72 hours after seeding. In the presence of 100 or 50% of aSF, no cells were able to attach (Fig. 1, B and C). Cell attachment was substantially improved at the SF level at 10% and further enhanced at 0%. To evaluate the effect of aSF on cell proliferation, acridine orange–labeled cells were seeded at 3000 cells/cm^2 in GM supplemented with or without 10% aSF, and cell proliferation was monitored for 14 days. Significantly less proliferation was seen in the aSF group after 3 days, and this lack of proliferation remained consistent for the whole culture period (Fig. 1, D and E). Cells cultured in GM alone continued proliferating until day 4 when they began to reach confluency and proliferation plateaued. Evaluation of senescence-associated β-galactosidase (SA-βgal) activity, detectable at pH 6.0, permits the identification of senescent cells. More than 40% of cells cultured in the presence of 10% aSF stained positive for SA-βgal activity in comparison to less than 10% of cells cultured in GM alone showed positivity for SA-βgal activity (Fig. 1, F and G).

The synovial environment in OA patients induces fibrosis of SF-derived cells

One of the most crucial aspects of a progenitor cell′s contribution to tissue repair includes its ability to differentiate and produce functional de novo extracellular matrix (ECM). Therefore, the SF-derived cells′ ability to undergo chondrogenic differentiation and produce cartilaginous ECM was next evaluated. For this, cells were seeded as microspheroids of 150 cells per spheroid for spontaneous aggregation in chondrogenic medium (CM) alone or supplemented with 10% aSF. Cells cultured in CM showed spontaneous aggregation after 24 hours (fig. S1A), with a general trend in spheroid diameter decrease after 7, 14, and 21 days, reflecting spheroid contraction as a sign of tissue maturation (fig. S1B). The supplementation of aSF markedly delayed the cells′ ability to undergo spontaneous aggregation and induced floating of the spheroids after 24 hours, leading to the formation of floating macrospheroids with the majority of microtissues fused (fig. S1, A and B). Histology for hematoxylin and eosin (H&E) on CM spheroids displayed a rounded cellular morphology similar to articular chondrocytes, embedded within a dense ECM (Fig. 1H). However, the supplementation of aSF induced a morphology resembling fibroblasts embedded in a loose and faint eosin-stained ECM indicative of fibrosis, further supported by the presence of a fibrotic connective tissue compartment including fibrous cords. These findings were further supported upon morphological macroanalysis by Picrosirius red staining and scanning electron microscopy (SEM) imaging, which confirmed impaired collagen organization and the formation of fibrotic structures upon stimulation with SF from OA patients (fig. S2). Evaluation of Alcian blue (AB), a basic cationic dye that stains proteoglycans and type II collagen blue with the stain intensity proportional to the glycosaminoglycan (GAG) content in the cartilage tissue, confirmed cartilaginous ECM production in the CM group, while a lack of proteoglycans was evident in the SF group (Fig. 1I). Quantification of AB$^+$ area confirmed a significant reduction in aSF samples compared to controls (Fig. 1J). Next, immunohistochemistry (IHC) for collagen type 2(COLL2)/COLL1, and lubricin confirmed a structure resembling the articular cartilage unit in CM samples with COLL2$^+$ area in the center of the spheroid, surrounded by a lubricin$^+$ core and a complete absence of COLL1$^+$ tissue (Fig. 1K). However, in spheroids cultured in aSF, the center of the spheroid showed positive for lubricin, the mid-zone limited COLL2$^+$, while the outer core showed COLL1$^+$. Upon quantification of the ratio COLL2/COLL1, over a 10-fold reduction was seen in aSF samples, while a twofold decrease in lubricin$^+$ was confirmed in aSF samples (Fig. 1L). To investigate how the aSF stimulation affected collagen morphology and distribution, spheroids were stained for Picrosirius red, followed by visualization under polarized light. This confirmed an impaired collagen production and distribution, where aSF stimulation induced a fibrotic structure typical of collagen type 1 fibers (fig. S2A). The underlying mechanism of the impaired cartilaginous ECM production could be linked to mRNA transcriptional events. Analysis of target genes confirmed over a 10-fold reduction in the expression of the master chondrogenic transcription factor sex-determining region of the Y (SRY)–box transcription factor 9 (*SOX9*) and the gene proteoglycan 4 (*PRG4*) encoding lubricin, upon aSF stimulation (Fig. 1M). Combined, these findings suggest that the impaired ability by SF-derived cells to contribute to tissue repair is due to a transcriptional dysregulation induced by factors present in the SF of OA patients.

Healthy articular chondrocytes dedifferentiate in SF from OA patients

To evaluate whether the impaired differentiation induced by aSF supplementation was strictly seen in SF-exposed cells, the effect on healthy articular chondrocytes (hACs) was next investigated. For this, hACs were seeded for three-dimensional (3D) culture in CM with or without 10% SF. Spontaneous aggregation was monitored by bright-field imaging, and differentiation was evaluated by histology, IHC, and mRNA transcript analysis. All groups formed spheroids after 24 hours of culture (Fig. 2A and fig. S2). After 72 hours, SF-cultured spheroids started floating with some fusing

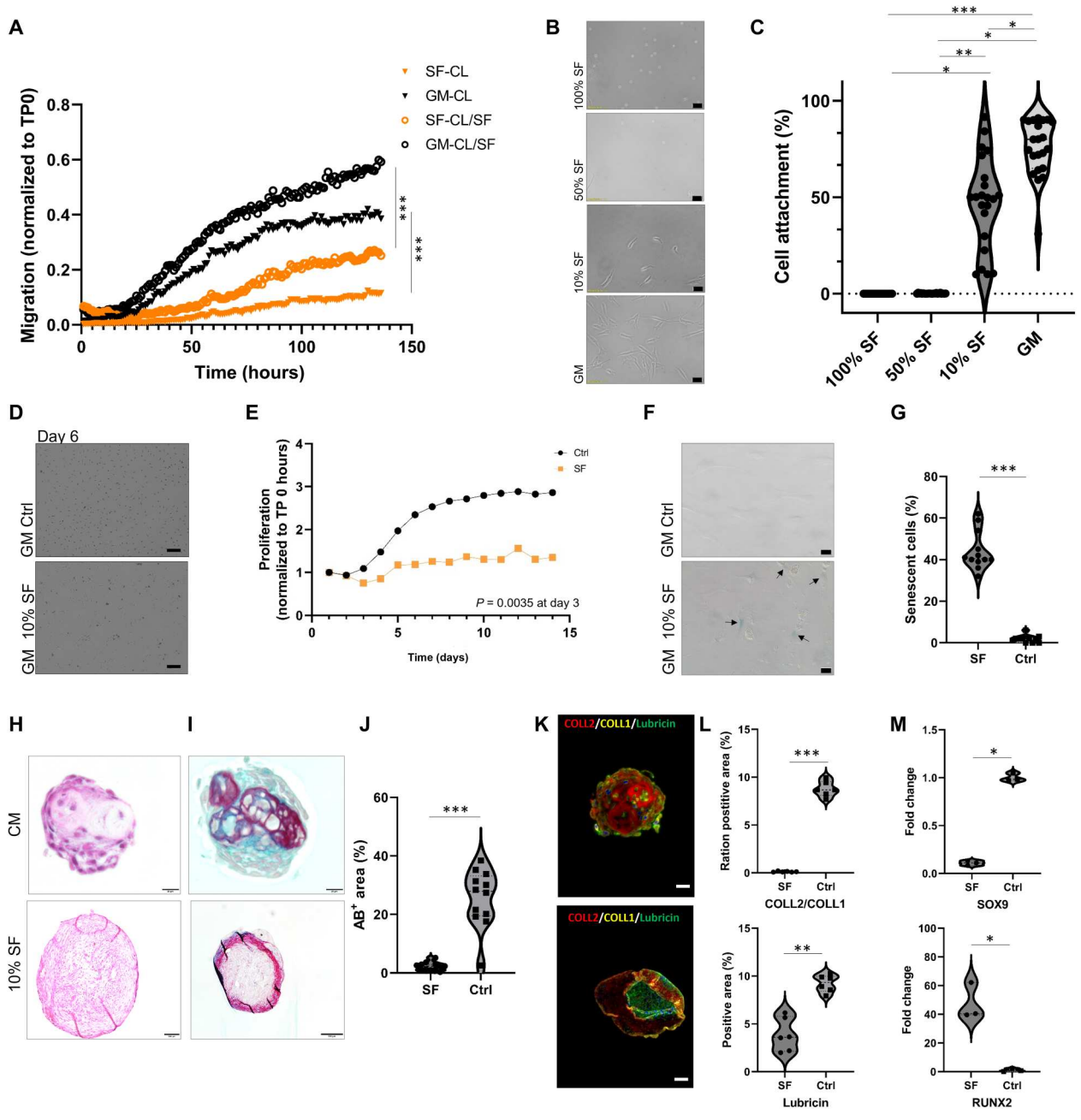

Fig. 1. SF from OA patients inhibits SF-derived cells' ability to participate in tissue regeneration. SF-derived cells were investigated in vitro for their ability to contribute to processes crucial for tissue regeneration in the presence or absence of aSF. Cells were seeded in GM with or without SF as migration medium, with CL or CL with SF as an attractor (**A**). For cell attachment, cells were seeded in GM with 10 to 100% SF, and attachment was investigated after 72 hours (**B**), followed by quantification (**C**). Cell proliferation in GM or GM supplemented with 10% SF was investigated by imaging (**D**) and quantification (**E**), followed by staining for SA-βgal (**F**) and calculation of percentage of SA-βgal$^+$ cells (**G**). Histology was performed after 21 days of three-dimensional (3D) culture in chondrogenic medium (CM) alone or supplemented with 10% aSF to evaluate general tissue morphology by hematoxylin and eosin (H&E) (**H**) and cartilaginous extracellular matrix (ECM) by Alcian blue (AB) (**I**) and subsequent quantification of AB$^+$ area (**J**). Immunohistochemistry (IHC) for COLL2, COLL1, lubricin, and 4′,6-diamidino-2-phenylindole (DAPI) as nuclear dye confirmed impaired ECM formation upon aSF stimulation (**K**). Quantification confirmed impaired COLL2/COLL1 ratio and lubricin$^+$ area in aSF stimulated samples (**L**). mRNA transcript analysis confirmed impaired *SOX9* and *PRG4* expression in aSF stimulated cells (**M**). Data are represented as individual data points: **P* < 0.05, ***P* < 0.01, and ****P* < 0.001. Significance in (A) and (E) from 24 hours and 3 days, respectively. Scale bars, 20 μm (B), 100 μm (D), 20 μm (F), and 50 μm (H, I, and K). TP0, time point 0 hours.

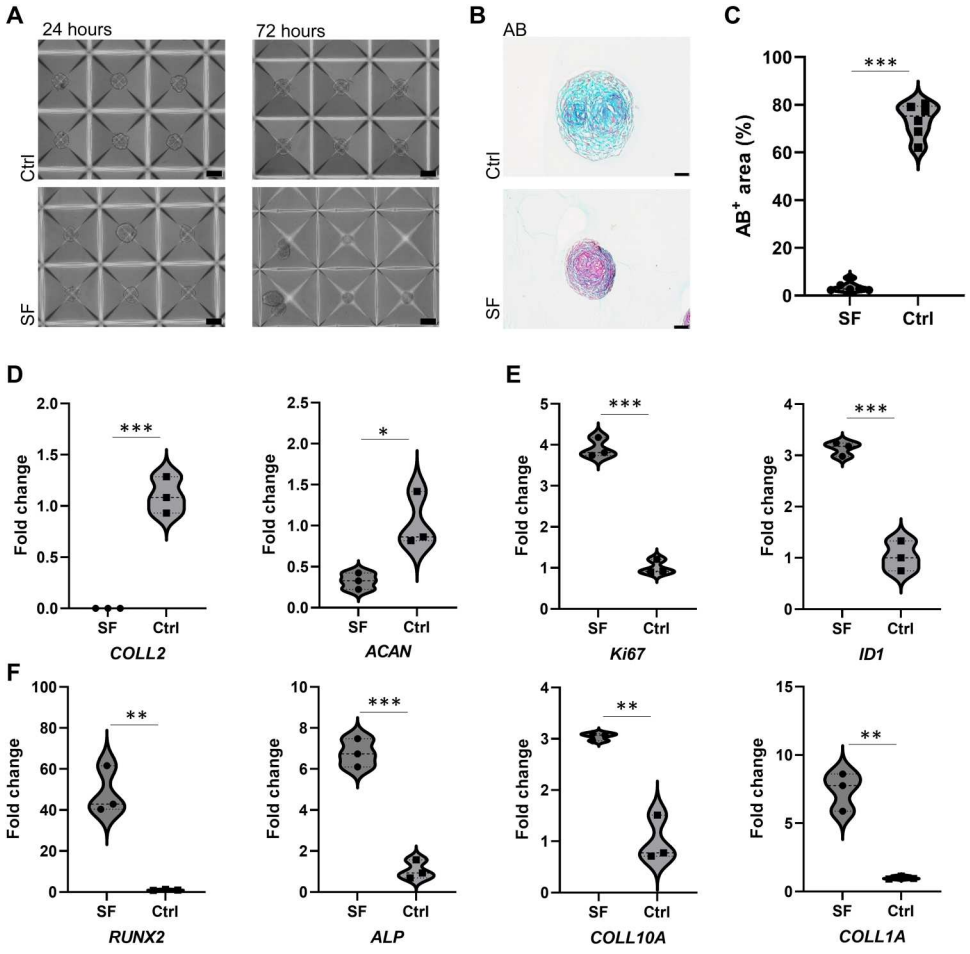

Fig. 2. SF from OA patients induces fibrosis in articular aggregates. Bright-field images of hAC 24 and 72 hours after seeding for spontaneous aggregation (**A**) and histology by AB after 10 days of stimulation (**B**) with subsequent quantification (**C**). mRNA transcript analysis for markers for articular chondrocytes (**D**), proliferation and Smad-dependent BMP signaling (**E**), and marker for endochondral bone formation (**F**). Data are represented as violin plots showing the probability density of the data: **P* < 0.05, ***P* < 0.01, and ****P* < 0.001. Scale bars, 10 μm (A) and 100 μm (B).

and formation of larger macrostructures. This phenomenon worsened with time (fig. S2, A and B). A few of the spheroids from the CM group fused because of movement of the plate during medium change but remained on the bottom of the well by ECM density. Histology for AB confirmed a GAG rich matrix in CM-stimulated hACs. In contrast, an impaired 80-fold reduction in GAG production was seen in SF samples (Fig. 2, B and C, and fig. S2). The induction of fibrotic ECM by SF stimulation of the hACs was further confirmed by SEM analysis (white arrows) and altered Picrosirius red staining under polarized light (white arrows; fig. S2, C and D). mRNA transcript analysis confirmed a chondrogenic lineage in the CM-cultured hACs depicted by *COLL2A* and Aggrecan (*ACAN*) expression, which was completely impaired in SF-cultured cells (Fig. 2D and fig. S2, E and F). Over a four- and threefold elevated expression of the proliferative marker *Ki67* and the canonical bone morphogenetic protein (BMP)–signaling marker inhibitor of differentiation 1 (*ID1*), respectively, was seen in SF-stimulated samples (Fig. 2, E to G). Furthermore, SF-stimulated samples displayed increased expression of dedifferentiation markers. This was reflected by a 20-fold elevated expression of the ECM marker *COLL10A*, expressed by hypertrophic chondrocytes. In addition, an eightfold elevated expression of the osteogenic transcription factor Runt-related transcription factor 2 (*RUNX2*) was seen. Furthermore, a threefold increased expression of the gene encoding alkaline phosphatase (ALP), essential for mineralization of newly formed osteoid, in combination with a 10-fold elevation of the bone ECM marker *COLL1A*, was depicted in SF-cultured samples (Fig. 2F). Together, these findings further confirm the fibrotic nature of SF isolated from OA patients, as indicated by dedifferentiation in healthy hACs upon stimulation.

The SF represents a pro-inflammatory environment

To understand what factors in the SF might be responsible for the induced dedifferentiation of hACs and impaired functionality of SF-derived cells, cytokine and protein profiling were performed. While the specific cytokine secretory profile differed between SF samples isolated from OA patients, a significantly higher expression of the pro-inflammatory cytokines, interleukin-17A (IL-17A) and IL-6, was seen compared to healthy controls (Ctrl) (Fig. 3A). No difference in the concentration of interferon-γ (IFN-γ) or tumor necrosis factor–α (TNF-α), cytokines involved in healthy and diseased tissue homeostasis, respectively, was observed. However, a clear, reduced

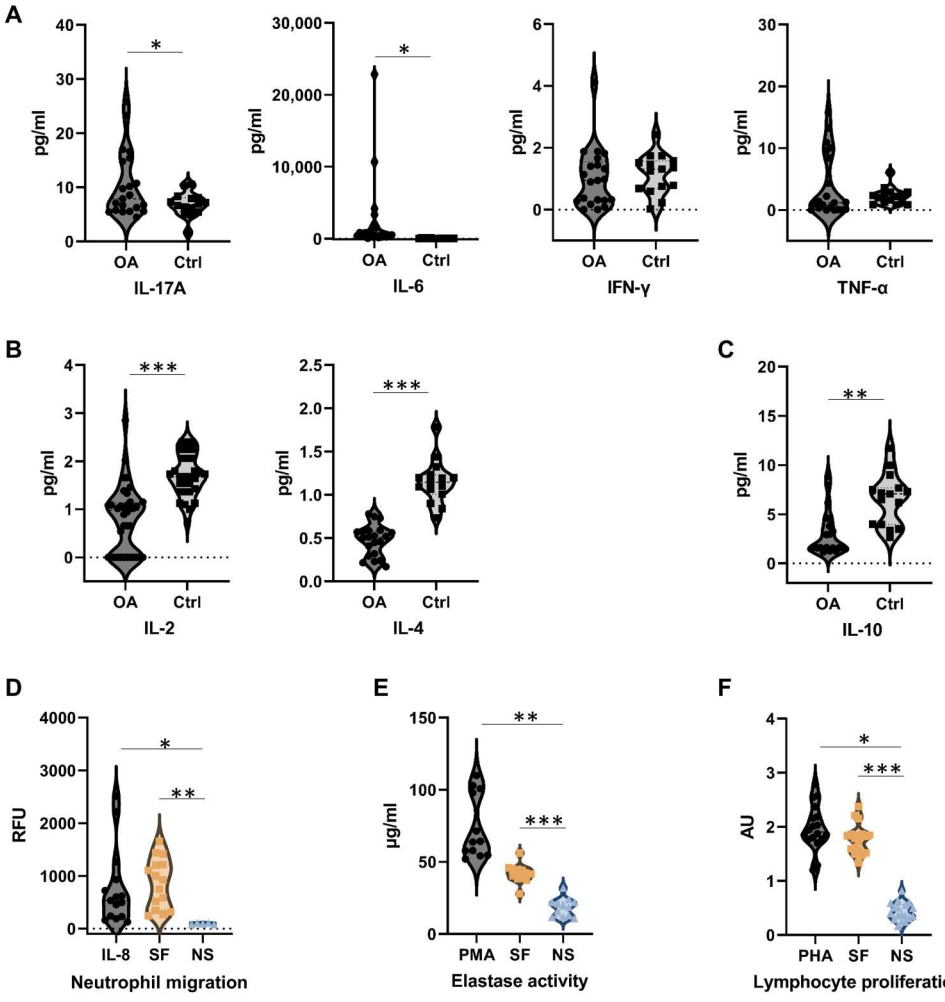

Fig. 3. SF from OA patients contains proinflammatory cytokines and stimulates inflammatory cells from healthy donors in a pro-inflammatory manner. Cytokine profiling of SF from OA patients and healthy controls for pro-inflammatory cytokines IL-17A, IL-6, IFN-γ, and TNF-α (**A**), cytokines secreted by the adaptive immune system IL-2 and IL-4 (**B**) and anti-inflammatory cytokine IL-10 (**C**). Mononuclear cells (MNCs) from healthy donors were isolated to evaluate the effect of SF from OA patients on neutrophil migration (**D**), neutrophil elastase activity (**E**), and lymphocyte proliferation (**F**). Data are represented as violin plots showing the probability density of the data: **P* < 0.05, ***P* < 0.01, and ****P* < 0.001. AU, absorbance units.

concentration of the pro-regenerative and anti-inflammatory markers IL-2 and IL-4 was seen between SF from OA patients and control SF samples (Fig. 3B). IL-10 is mainly secreted by macrophages and lymphocytes and is a key anti-inflammatory cytokine that can inhibit pro-inflammatory responses of both innate and adaptive immune cells (*10*). Analysis of IL-10 in SF displayed reduced levels in fluid from OA patients compared to controls (Fig. 3C). To further evaluate the effect of SF derived from OA patients, neutrophils and macrophages were isolated from healthy donors to study the effect of SF in pro-inflammatory events, such as neutrophil migration, neutrophil elastase activity, and macrophage proliferation. IL-8 induced neutrophil migration, as also seen in SF stimulated samples (Fig. 3D). Meanwhile, there was over a 2000-fold increased migration in the SF stimulated group compared to nonstimulated (NS) controls (Fig. 3D). Phorbol myristate acetate (PMA) was used as a control to induce neutrophil elastase activity. Both SF and the PMA induced significant neutrophil elastase relative to the NS group (Fig. 3E). In a final step, phytohaemagglutinin (PHA) was used to activate pro-inflammatory lymphocyte proliferation (*11*). Significant lymphocyte proliferation and pro-inflammatory cytokine secretion was seen upon PHA or SF stimulation, while limited effect was observed in NS cells or on anti-inflammatory and pro-regenerative cytokines (Fig. 3F and fig. S3).

Functional tissue regeneration inspired the development of an immunomodulatory cell treatment

The detailed characterization of SF from OA patients indicated a clear pro-inflammatory response to the SF. Our in vitro findings suggested that this pro-inflammatory environment was caused by an imbalance in the activation of pro-inflammatory and pro-regenerative immune cells, resulting in fibrosis and the onset and progression of OA. This is in line with previous literature where an imbalance in the infiltration and residence of pro-inflammatory cells are seen in the synovial joint during OA initiation and progression (*12*–*14*). To test this in vivo, an immunomodulatory cell-based treatment was developed with the goal of mimicking and promoting

the crucial events observed during functional tissue regeneration. Mononuclear cells (MNCs) and adipose tissue were isolated as a source of T cells and aMSCs, respectively (Fig. 4A). The MNCs were activated for cartilage tissue by culture in an activation medium containing CL and inhibitors for pro-inflammatory cells (Fig. 4B). This activation generated CATs that were then cocultured with in vitro expanded aMSCs for 24 hours to induce chondrogenic priming of the aMSCs (Fig. 4C). This cell treatment, upon intra-articular injection into an OA knee (Fig. 4D), tests the hypothesis that the tissue-specific activation of pro-regenerative T cells activates the chondrogenic program in the aMSCs and further steer these locally recruited progenitor cells and neighboring chondrocytes to accomplish functional tissue repair of deteriorated cartilage and inflammation (Fig. 4E).

Cartilage-activated immune cells induce chondrogenic differentiation in adipose-derived progenitor cells

Flow cytometry was used to characterize the activated CAT cell population compared to the initial MNC population. CD4, expressed by naïve T cells, displayed a twofold decrease in the CATs (Fig. 5A). Next, the characterization confirmed a 1.2-fold increased expression of CD3, a multimeric protein complex and a defining feature of the T cell lineage, in the activated CAT population combined with a twofold elevated expression of CD69, expressed by activated T cells (Fig. 5A). A twofold increased expression of CD25, a marker for T regulatory cells, was also observed (Fig. 5A). To investigate the secretory profile of the activated CATs, cytokine profiling was carried out on the conditioned medium isolated from activated CATs and nonactivated MNCs. A 40- and 10-fold elevated concentration of the pro-regenerative cytokines IL-10 and IL-2, respectively, was detected in the CATs compared to conditioned medium from nonactivated MNCs (Ctrl; Fig. 5B and fig. S4A). Meanwhile, no difference was detected between the concentration of pro-inflammatory cytokines IL-6 and IL-17A between CATs and Ctrl (Fig. 5C). Because the analysis of the cell surface expression and secretory profile of the activated CATs indicated a clear shift in cellular identity, mRNA transcript analysis was performed. Analysis of *IL17A* supported findings from the cytokine profiling with a 10-fold decrease in gene expression in CATs as compared to nonactivated MNCs (Fig. 5D and fig. S4A). The cytokine findings were also confirmed with the expression for the anti-inflammatory cytokine *IL10* and *TNFα* (Fig. 5E). A 1.4-, 5.5-, and 2.5-fold elevated expression of the chondrogenic inducers *TGFβ1*, *BMP-2*, and *COMP* was depicted in the activated CATs, indicative of a mechanism for their ability to induce chondrogenic priming of progenitor cells (Fig. 5F). mRNA analysis of aMSCs after 0, 24, 48, 72, and 96 hours of coculture with the CATs further supported the CAT-induced chondrogenic differentiation. An immediate, elevated expression was found in the early chondrogenic commitment marker *GDF5* and the master chondrogenic transcription factor *SOX9*, upon 24 hours of coculture (Fig. 5G). Analysis of *TGFβ1* displayed a decreased expression after 24 hours of coculture, followed by an increased expression after 72 and 96 hours of coculture. This gradually increased expression was further supported by Dickkopf

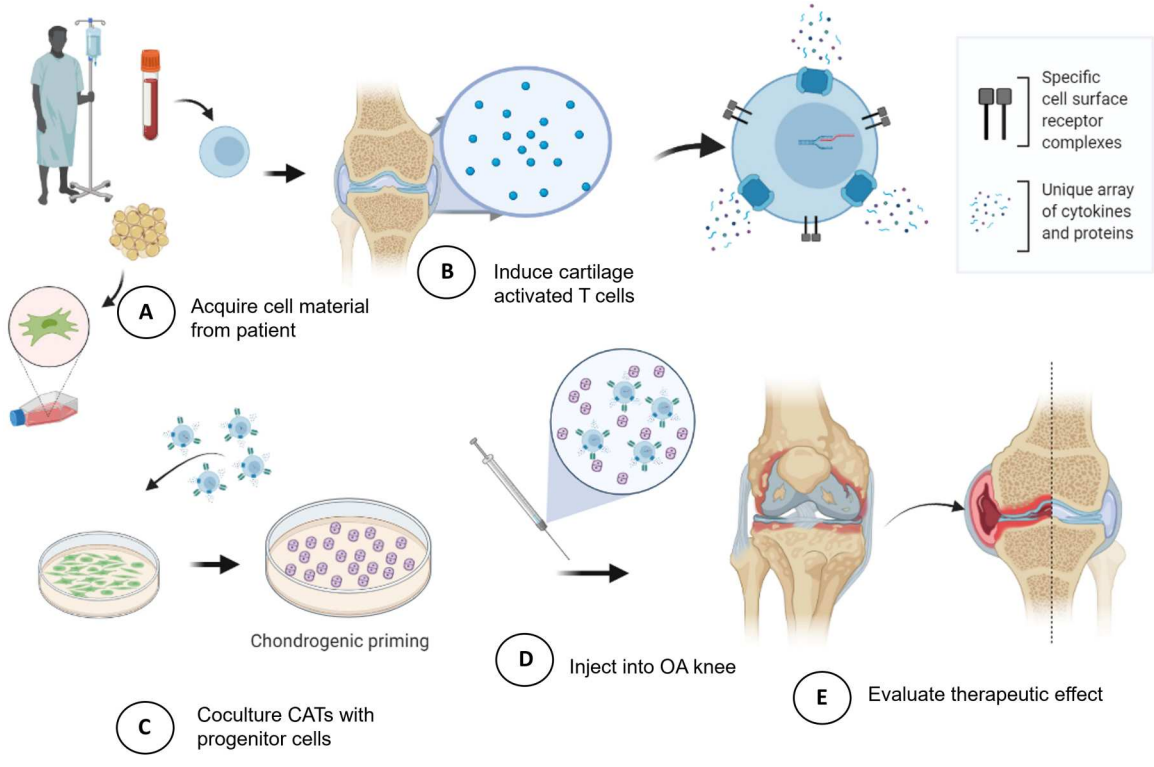

Fig. 4. Development of an immunomodulatory and pro-regenerative cell treatment. MNCs are isolated from blood or spleen, while aMSC are isolated from adipose tissue and expanded in vitro (**A**). The MNC are activated toward cartilage tissue and stimulated with inhibitors for anti-inflammatory properties for 72 hours to become CATs (**B**). Next, the CATs are added to the in vitro expanded aMSCs for a 24-hour coculture to induce chondrogenic priming of the aMSCs (**C**) followed by intra-articular injection (**D**) for the treatment of OA for potential restoration of joint homeostasis (**E**).

A

Marker	MNC (%)	CAT (%)
CD3	4.7	5.5
CD4	17.3	8.2
CD25	2.0	3.4
CD69	1.4	2.1
CD68	7.5	9.7

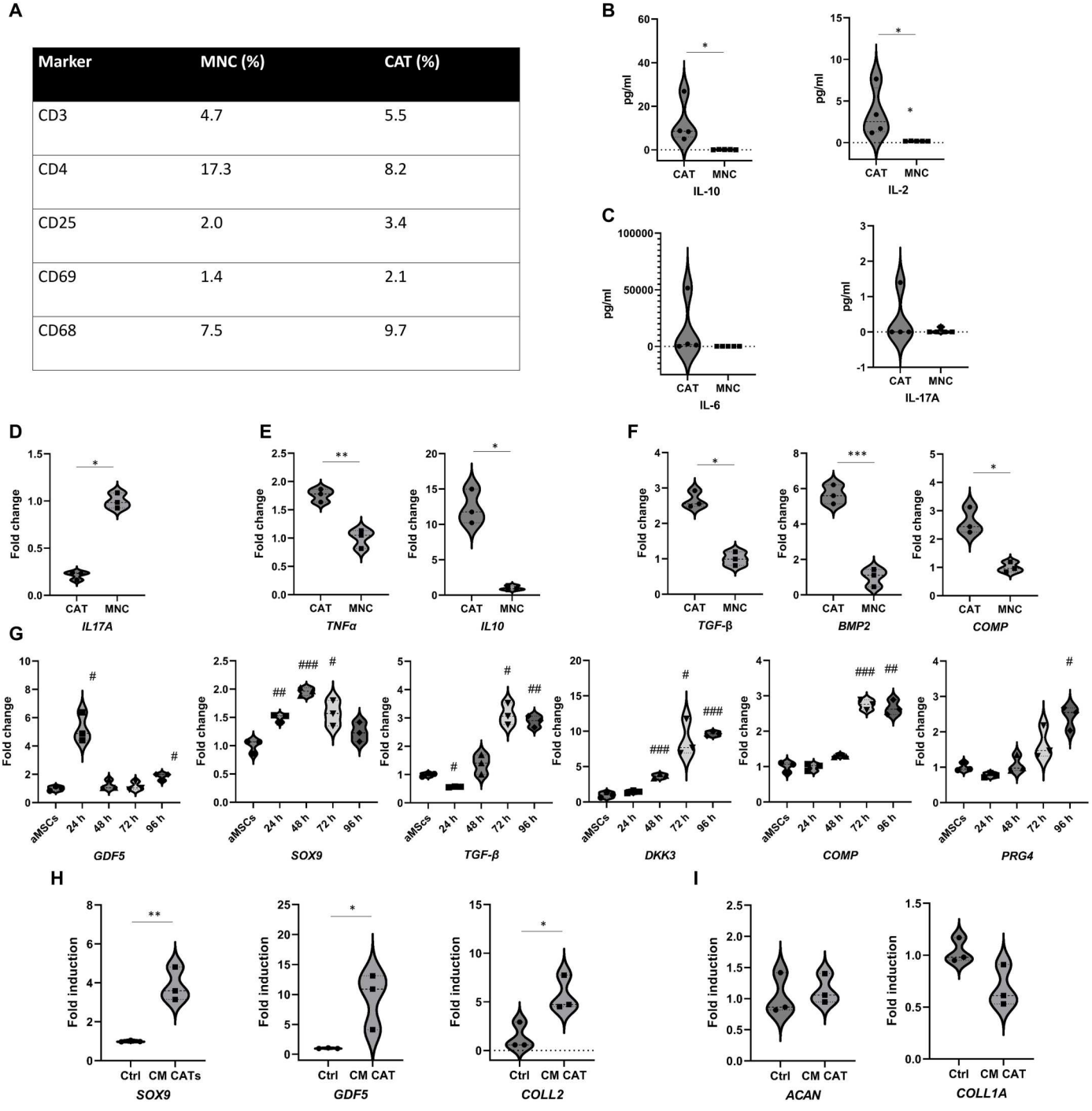

Fig. 5. Characterization of an immunomodulatory cell-based regenerative treatment. The expression of cell surface markers upon activation of MNCs to CATs was investigated by flow cytometry (**A**). Cytokine profiling for pro-regenerative (**B**) and pro-inflammatory (**C**) cytokine markers. mRNA transcript analysis after 72 hours of CAT activation for pro-inflammatory (**D**), anti-inflammatory (**E**), and proteins inducing chondrogenesis (**F**). mRNA transcript analysis was used to investigate the temporal mechanism of CAT-induced chondrogenic differentiation of aMSC (**G**). The conditioned medium from activated CATs (CM CAT) was investigated for the ability to stabilize the articular chondrocyte phenotype when added to standard CM (**H**) and to protect against dedifferentiation (**I**). Data are represented as individual data points or violin plots showing the probability density of the data: *P < 0.05, **P < 0.01, ***P < 0.001, and ****P < 0.0001; #P < 0.05, ##P < 0.01, and ###P < 0.001 to time point 0 hours.

WNT signaling pathway inhibitor 3 (*DKK3)* expression, a molecule with a protective effect on TGFβ-induced cartilage integrity by preventing proteoglycan loss in OA (*15*). Next, analysis of the glycoprotein cartilage oligomeric matrix protein (*COMP*), crucial for cartilage ECM structure and load-bearing function, was assessed. After 48 hours of coculture, a 1.3-fold increased expression was seen and enhanced at 72 hours to over a 2.7-fold elevated expression. This progressive, increased elevation in expression was also observed for *PRG4*, the gene encoding lubricin. Here, a 1.7-fold elevated expression was seen at 72 hours, which increased to a 2.5-fold at 96 hours (Fig. 5G and fig. S3B). To further investigate how the secretory profile of the activated CATs may affect chondrocytes in the defect environment, healthy human articular chondrocytes were seeded for spheroid formation and cultured in standard CM with or without 10% of conditioned media from the activated CATs (CM CAT). mRNA transcript analysis confirmed that over 4- and 15-fold elevated expression was seen in *SOX9* and *GDF5*, respectively (Fig. 5H). While no difference in *ACAN* expression was observed between CM- and CM CAT–stimulated hACs, over a fivefold increase in *COLL2* was confirmed in CM CAT–stimulated hACs. Combined, these findings confirm that cartilage activation of CATs induces an ability to initiate and steer stable chondrogenic differentiation of progenitor cells upon coculture. Furthermore, CATs produce cytokines and proteins that further stabilize the chondrogenic phenotype of articular chondrocytes in vitro.

Immunomodulation of OA in a preclinical model leads to restored joint homeostasis

To evaluate the regenerative effect of the immunomodulatory cell treatment in cartilage-specific fibrosis, a chemically induced OA model in rat was used. Monosodium iodoacetate (MIA) is a glycolytic inhibitor that causes behavioral, histological, and biochemical changes that resemble human OA and its associated joint pain upon local injection (*16*, *17*). MIA was injected in the right hind knee of 9-week-old female Lewis rats (Fig. 6A). One week after injection, initiation of cartilage deterioration depicted by reduced AB stain and impaired collagen structure in the articular surface demonstrated by Picrosirius red was observed in MIA-injected knees but not in vehicle controls (Fig. 6B and fig. S5A). Next, CATs, aMSC, a 24-hour coculture (CoC) between aMSCs and CATs, or nontreated vehicle control (Ctrl) was injected intra-articularly 1 week after MIA injection. Evaluation by AB and Picrosirius red staining for cartilage deterioration 3 weeks after cell injection confirmed severe cartilage degradation in nontreated MIA-injected knees (Fig. 6C and fig. S5B). Limited articular cartilage regeneration was seen upon injection of aMSCs alone, while a fourfold elevated AB-positive ECM was detected in the CAT-treated group (Fig. 6, C and F, and fig. S5B). The cocultured group induced regeneration of the articular unit similarly to the vehicle control group (Fig. 6, C to F, and fig. S5B). To assess the quality of the degenerated or regenerated cartilage, IHC for COLL2, COLL1, and lubricin was performed (Fig. 6D and fig. S6). Further confirming findings from the AB staining, aMSC treatment alone did not improve $COLL2^+$ matrix formation. Instead, the presence of $COLL1^+$ ECM could be confirmed in the articular cartilage unit. While limited $COLL2^+$ ECM was detected in CAT-treated animals, the presence of $COLL2^+$ ECM was similar in the CoC-treated group and vehicle control, confirming articular cartilage regeneration. Quantification of the $lubricin^+$ layer displayed limited positive staining in the nontreated and aMSC groups, while a twofold elevated level $lubricin^+$ area was seen in the CAT and CoC groups (Fig. 6, D and H, and fig. S6). The Osteoarthritis Research Society International (OARSI) scoring system was developed as a histologic scoring system that can be applied universally to various OA models (*13*, *14*). The highest score for cartilage degeneration was detected in nontreated joints with a score of 4.17 ± 0.75. Limited improvement was seen in aMSC- and CAT-treated animals, which scored 3 ± 1.08 and 2.33 ± 0.82, respectively, while the CoC group scored 0.67 ± 0.82, reflecting near full regeneration of the deteriorated cartilage (Fig. 6E). In addition, IHC for SRY confirmed contribution of the injected male cells to the restored joint homeostasis in the female animals (fig. S7). As the synovial membrane structure and composition reflect joint health and function as an immunomodulatory hub for the synovial joint, treatment group effects on the synovial membrane after MIA injections were investigated. For this, a synovial membrane fibrosis score was used on the basis of the cell layer thickness of the synovial membrane (black arrows), the presence of vascularized connective tissue (blue arrows), edematous subintimal layer (green arrows), and inflamed intimal layer (gray arrows), as indicative markers of synovial inflammation. Similarly to the evaluation of articular ECM regeneration, the CoC group displayed the strongest ability to reverse fibrosis in the synovial membrane. This suggested that the combined cell treatment did not only function to directly regenerate the deteriorated cartilage but also affected the inflamed membrane by steering its pro-inflammatory status toward a more pro-regenerative environment (Fig. 6, I and J).

Intra-articular injection of an autologous immunomodulatory cell treatment improves pain, quality of life, and joint status in a clinical compassionate use study

To evaluate clinical efficacy, a compassionate use study was conducted in nine patients with confirmed knee OA graded to 3-4 by symptoms including (i) pain, reduced function in daily life, reduced function in sports, recreational activities, and reduced quality of life according to the Knee Injury and Osteoarthritis Outcome Score (KOOS) scale (*18*); (ii) conformational x-ray; and (iii) magnetic resonance imaging (MRI). All patients received one or two intra-articular injection(s) of autologous CoC treatment (Fig. 7A). Efficacy was monitored through KOOS evaluation and MRI before and after treatment, and a biopsy from one patient could be harvested (Fig. 7 and fig. S8). Upon treatment, an increase in quality of life was confirmed ($P = 0.078$; Fig. 7B). This could be linked to an elevation in functional daily living ($P = 0.007$) (Fig. 7C), improvement in function during sports and recreational activities ($P = 0.0153$; Fig. 7D), an increase in symptom improvement ($P = 0.0031$; Fig. 7E), and increase in pain improvement ($P = 0.0039$; Fig. 7F). MRI analysis before treatment in a 30-year-old athlete who had failed conservative therapy of rest, physical therapy, nonsteroidal anti-inflammatory drugs (NSAIDs), and steroid injections indicated OA based on depicted focal osteochondral lesions in the weight-bearing regions of the lateral femorotibial and posterior lateral compartment (Fig. 7G). MRI approximately 1 year after treatment indicated restoration of the articular cartilage unit and distinct decrease in subchondral edema (Fig. 7H). One patient suffered from knee OA due to anterior cruciate ligament (ACL) rupture, as depicted by degenerated cartilage in obtained MRI before treatment. Diffuse cartilage substance loss and focal superficial cartilage damage were confirmed in weight-bearing regions of the medial

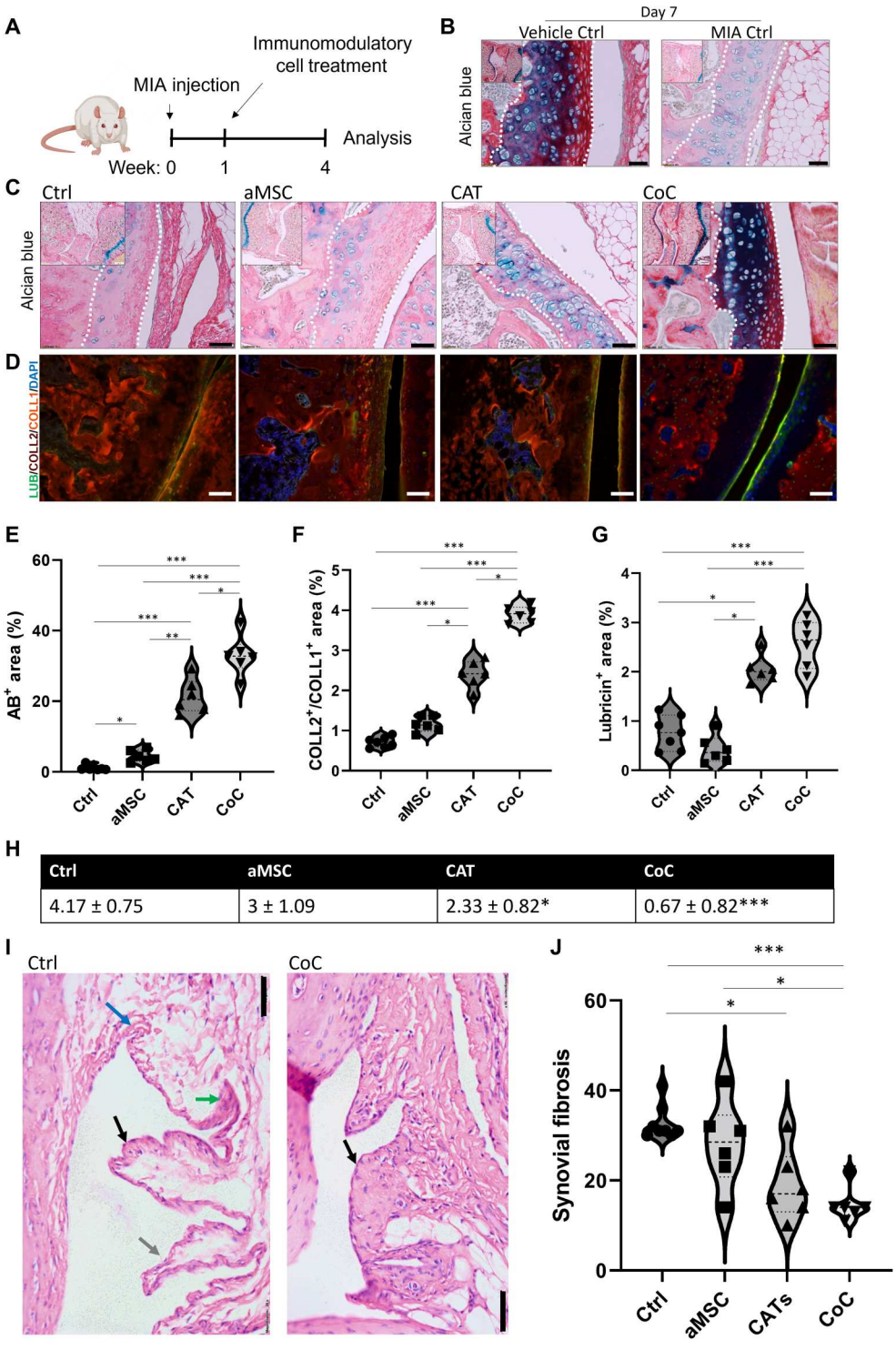

Fig. 6. Functional articular and synovial membrane regeneration upon chemically induced OA in rat. MIA was injected intra-articularly in female rat followed by injection of aMSCs, CATs, or CoC 1 week later and final histology at week 4 (**A**). Histology by AB confirmed the onset of cartilage deterioration 1 week after MIA injection, but not in vehicle control (**B**). ECM characterization 3 weeks after cell injection for AB confirmed a treatment-specific response in GAG regeneration (**C** and **E**) and COLL2, COLL1, and lubricin production (**D**, **F**, and **G**). Combined, these findings gave treatment group–specific OARSI scoring for articular cartilage degeneration with statistical difference to nontreated control (**H**). Characterization of fibrosis in the synovial membrane by H&E staining based on cell layer thickness of the synovial membrane (black arrows), vascularized loose connective tissue (blue arrows), edematous subintima layer (green arrow), and inflamed intima layer (gray arrow) (I) and synovial fibrosis score between the different treatment (**J**). Data are represented as individual data points or violin plots showing the probability density of the data: *$P < 0.05$, **$P < 0.01$, and ***$P < 0.001$. Scale bars, 50 μm.

A

#	Sex	Age	Affected knee	OA degree	Number of implants	Associated to arthroscopy	OA etiology
01	M	35	L	4	1	Yes	Traumatic
02	M	61	L-R	4-4	2	No	Inflammatory
03	M	69	L-R	4-4	1	Yes	Degenerative
04	F	78	L-R	4-4	2	No	Traumatic
05	M	58	L-R	3-3	2	No	Traumatic
06	M	91	L-R	4-4	2	No	Traumatic
07	M	49	L-R	3-2	1	No	Traumatic
08	F	55	L-R	3-3	1	No	Degenerative
09	F	51	L-R	4-4	1	No	Degenerative

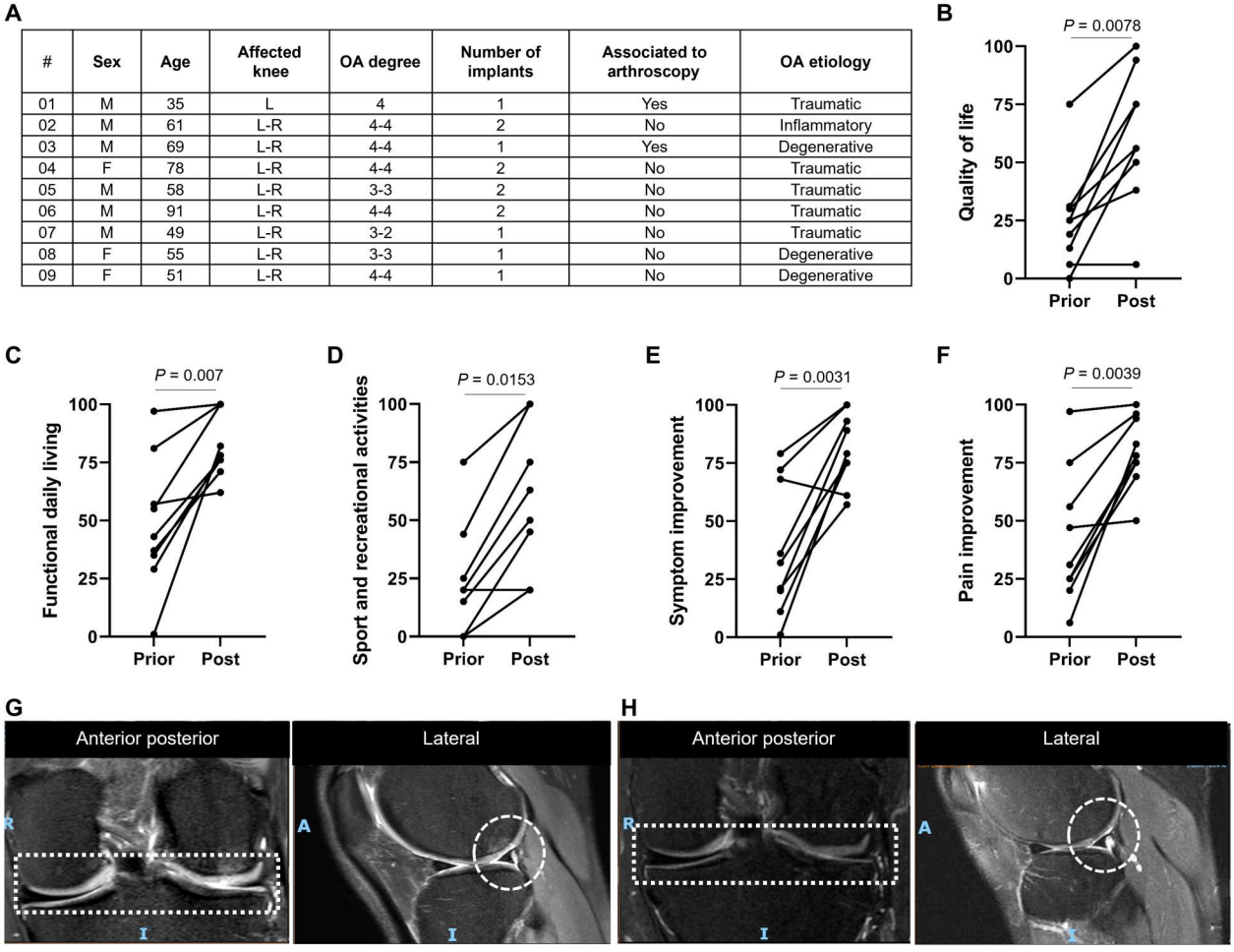

Fig. 7. Improved articular cartilage regeneration upon autologous treatment of trauma induced OA in a clinical compassionate study. Recruited patients for a compassionate use study included mainly trauma or degenerative OA, followed by one or two intra-articular injections of autologous CoC treatment (**A**). Follow-up studies 1 year after the last injection led to improved total KOOS score based on quality of life (**B**), function in daily living (**C**), improved participation in sports and recreational activities (**D**), symptom (**E**), and pain (**F**) improvement. MRI analysis before treatment in this young athlete who had failed conservative therapy of rest, physical therapy, NSAIDs, and steroid injections indicated OA based on depicted focal osteochondral lesions in the weight-bearing regions of the lateral femorotibial and posterior lateral compartment (**G**). MRI approximately 1 year after treatment indicated restoration of the articular cartilage unit and distinct decrease in subchondral edema (**H**).

and lateral compartments (fig. S8A). When this patient received intra-articular injection of autologous CoC (without ACL reconstruction), restoration of the articular cartilage unit and distinct separation from the subchondral bone were obtained (fig. S8, A and B). Together, these findings suggest that an imbalance between the activated pro- and anti-inflammatory immune cell populations steers the initiation, progression, and resolution of OA.

DISCUSSION

OA was recently identified by the U.S. Food and Drug Administration as an epidemic, a public health crisis affecting more than 520 million people worldwide, with no effective treatments available. The lack of reliable therapies is largely due to our limited understanding regarding the cause and underlying mechanism of OA pathophysiology. We herein report on the development of an immunomodulatory cell treatment, with the ability to restore joint homeostasis upon OA deterioration in human and rat. OA is a disease of the joint system, and the synovial membrane is a highly specialized connective tissue that lines the inner surface of the joint capsule. The membrane functions to (i) protect the joint, (ii) control the composition of the ECM and SF, (iii) provide progenitor and immune cells to maintain joint homeostasis, and (iv) supply mechanical support. In diseases such as OA, a clear change in the structure and composition of the synovial membrane is detected. The synovium may show substantial changes even before visible cartilage degeneration has occurred, including infiltration of MNCs, alteration in T cell subsets, thickening of the synovial lining layer, and altered production of inflammatory cytokines (*16*, *19*). Upon injury and during OA progression, the number of mesenchymal progenitor cells in the SF increases (*17*, *20*). This suggests that articular cartilage deterioration may induce a similar activation of progenitor cells from the local environment, as seen upon acute injuries (*9*). However, activated progenitor cells in the OA environment fail to heal the damage (*21*). In line with previous research, SF-derived cells in this investigation showed the potential

to proliferate in monolayer and to undergo chondrogenic differentiation in 3D culture conditions (*21*, *22*). However, when aSF was added to the assay medium, proliferation was impaired and cells became senescent, while cells under chondrogenic differentiation conditions dedifferentiated and became fibrotic with the addition of aSF. This phenomenon was not specific to SF-derived cells. When hAC isolated from healthy donors were cultured in SF from OA patients, dedifferentiation toward a fibrotic/osteogenic phenotype was observed. Furthermore, the SF-derived cells' ability to migrate and attach to tissue culture surfaces was confirmed. These processes were additionally impaired in the presence of aSF. While steric hindrance could be a potential cause for this (*22*), supplementation of hyaluronic acid at identical concentrations did not interfere with cell migration or attachment. On the basis of these initial findings, the transition to a pro-regenerative environment fails in the synovial OA joint because of the SF composition (*8*).

These discoveries confirmed the SF as a central site of inflammation during OA progression, and this is supported by previous findings (*22*, *23*). The initial stages of immune-mediated joint diseases such as OA are characterized by the influx of immune cells into the synovial compartment (*24*–*26*). Local activation of these cells in the synovial vasculature enables their transendothelial migration into the inflamed tissues, with leukocyte accumulation further potentiated by the up-regulation of pro-inflammatory cytokines (*22*). OA is thought to be initiated by stress or trauma that fails to be resolved, leading to a prolonged pro-inflammatory response resulting in fibrosis (*27*, *28*). As the disease progresses, it can be hypothesized that a local trauma signal is sent out by the affected tissue, leading to a constant secretion of signals to recruit neighboring progenitor cells to aid in tissue restoration and regeneration (*17*, *20*). However, the pro-inflammatory environment in SF impairs the progenitor cells' ability to regenerate healthy tissue.

Unfortunately, the majority of treatment alternatives for OA only focus on one aspect of the disease, e.g., to treat the pro-inflammatory environment, reduce the pain, or induce regeneration. The discoveries of this current investigation support the hypothesis that the pro-inflammatory environment in SF of OA patients is caused by an imbalance in the activation of pro-inflammatory and pro-regenerative T cells due to the initial tissue trauma. To test this, an immunomodulatory cell-based treatment was developed with the goal to mimic and promote crucial events seen during functional tissue regeneration. Specifically, a pro-regenerative tissue-specific T cell population was generated to override the negative impact of the OA-initiated pro-inflammatory cells and to promote homeostasis in the joint system. Furthermore, through tissue-specific activation, the activated cells would be able to steer chondrogenic differentiation of progenitor cells to aid in local regeneration upon intra-articular injection. A protocol was established for the activation of cartilage-targeted pro-regenerative T cells combined with adipose-derived progenitor cells for an autologous treatment. Upon coculture of the two populations, the progenitor cells would be primed (*29*), but not fully differentiated, since it may impair integration (*30*). These progenitor cells together with recruited cells from the local environment would be able to regenerate the damaged tissue with instructions from the activated T cells (*31*). It is currently understood that T cells are critical for orchestrating appropriate adaptive immune and tissue responses and for maintaining homeostasis in regulation to nonpathogenic antigens. T cell function is controlled in part by environmental signals, such as antigens. This targets the T cells toward the specific tissue that the antigen derived from (*32*). Recent reports argue that additional tissue-specific signals affect T cell differentiation and function (*33*). This suggests that the existing OA environment further steers local and recruited immune cells toward a pro-inflammatory status, leading to worsening conditions. At the same time, trauma signals recruit progenitor cells, resulting in impaired tissue regeneration and subchondral bone sclerosis. To overcome this, MNCs were activated in vitro to obtain a cartilage-targeted anti-inflammatory and pro-regenerative T cell population that can initiate chondrogenic differentiation of aMSCs in vitro and further steer tissue restoration in vivo. Once injected intra-articularly in a rat OA model, articular cartilage and synovial restoration was confirmed. A limited effect of injection of aMSCs or CATs alone was seen. These findings were in line with previous reports where aMSCs were injected at different time points following chemically induced OA in rats (*34*). In these studies, aMSC cell injection mainly led to short-term pain-suppressing effects, associated with the down-regulation of TNF-α in the synovium of OA knee joints. These results are further supported by others, suggesting that aMSC injection mainly attenuates articular cartilage degradation through a short-term immune-suppressing effect (*35*–*37*). This suggests that when aMSCs are injected alone, they first function to modulate the immune response. Hence, they have a limited effect on tissue regeneration. By injecting the cocultured product, the aMSCs are targeted to regenerate the articular cartilage, while the CATs steer the local environment and suppress the pro-inflammatory factors.

In the clinical setting, the cocultured immunomodulatory cell treatment was injected intra-articularly for compassionate use. In the nine included patients who received the treatment, improved quality of life, ability to participate in recreational activities, and reduced pain were seen. In parallel, articular cartilage regeneration was confirmed by MRI and histology. Limitations with our study include that the main findings were obtained in a rat OA model. Rat joint biology and mechanical properties differ from humans; these are crucial factors that play a role in OA biology, and in the future, models with natural OA development would be of benefit. Clinical improvements were obtained; however, this was only obtained in a small group of patients for compassionate use. Additional clinical studies are required to evaluate the outcome in a larger patient population and to evaluate dosage, timing, and potency of cells derived from donors with different health statuses. However, the reported findings herein demonstrated the crucial impact of a well-balanced immune environment for tissue homeostasis and functional repair. The presented findings can provide inspiration and directions for the treatment of effective and patient-specific immunomodulatory treatments with the ability to restore or regenerate damaged tissues and organs.

MATERIALS AND METHODS

Study design

This study was performed to evaluate whether the heterogeneous cell population present in the synovial environment lacks the capability to contribute to functional tissue repair or whether there is something in the environment that impairs their ability to do so. This objective was addressed by isolating SF from OA patients in

the early phase of disease initiation. Cells and the fluid portion were separated, and the cells were evaluated for their potential to undergo migration, attachment, proliferation, and chondrogenic differentiation in the absence or presence of aSF. Next, the obtained findings were used in the development of an immunomodulatory cell treatment. Sample size was determined by the investigators according to previous experimental procedures. The *n* numbers used in each experiment are indicated in the details for each experiment. For in vivo experiments, data from animals that died for non-experimental causes were excluded. Samples were assigned randomly to the experimental and control groups. Animal or sample allocation and data acquisition in vivo or ex vivo and scoring were performed in a blinded manner. Further experimental procedures are detailed in Supplementary Materials and Methods.

SF collection and processing

All work with SF collected from human patients was approved by the Wake Forest Baptist Medical Center Institutional Review Board (IRB; study ID: IRB00007586). Patients seeking medical care for joint discomfort or pain without any previous treatments were identified. All patients provided written informed consent before SF was collected. Approximately 3 to 20 ml of SF was obtained via arthrocentesis from the affected knees of 23 patients (11 males and 12 females; mean age, 55.6 ± 9.22 years). Upon collection, SF was centrifuged at 2000*g* for 30 min. Supernatant was aliquoted and stored at −80°C for further analysis. SF from five donors with no history of joint disease or arthritis and that tested negative for HIV 1 and 2, hepatitis C antibody, and hepatitis B surface Antigen was obtained from a commercial vendor (Articular Engineering, Northbrook, IL, USA). The 1-ml fluid samples were harvested postmortem from donors with no clinical history of joint disease or arthritis. Each sample was frozen immediately after collection, stored frozen at −80°C, and shipped on dry ice. Upon arrival, samples were immediately transferred to −80°C until further analysis.

Cell culture

SF-derived cells were isolated from the SF after centrifugation. Next, cells were washed in phosphate-buffered saline (PBS), followed by cell expansion in GM consisting of Dulbecco's modified Eagle's medium (DMEM)/F12 supplemented with 10% fetal bovine serum and 1% penicillin/streptavidin for three passages when they were used for the specific assays. Primary healthy human articular chondrocytes (PromoCell, Heidelberg, Germany) were cultured in chondrocyte media (PromoCell) to passage three when they were processed for assays.

Rat model of chemically induced OA

Twenty-five 8- to 9-week-old female Lewis rats were randomly assigned to one of three experimental groups. All animal procedures were performed in accordance with the National Institutes of Health *Guide for the Care and Use of Laboratory Animals* and with a protocol approved by the Institutional Animal Care and Use Committee at Wake Forest University Health Sciences (protocol number: A20-046). Table 1 describes the demographics of the groups, including the average start and end weights, along with the length of time of each animal within the study. Each animal's entry into the study was initiated by a 50-μl intra-articular injection of 0.2 mg of MIA into the right stifle joint to produce a rapid, degradative effect on the articular cartilage equilibrate to grade II to IV lesion (*38*–*40*). Four control animals were euthanized 7 days after MIA injection to document the degree of damage at the time of administration of the cell therapy. Three different cell treatments were provided: (i) CATs only, (ii) aMSCs only, and (iii) a 24-hour CoC of CATs and aMSC in a 4:1 ratio; control animals received PlasmaLyte without cells. For each experimental group, $n = 6$ was planned, but two animals failed recovery from anesthesia after MIA injection. The MNCs used for the CATs and adipose tissue used to isolate the aMSCs were obtained from donor male Lewis rats harvested before the beginning of the experiment. Because this strain is inbred, these cells were treated as an autologous graft. The experimental animals receiving cells were euthanized 21 days after cell therapy injections. At tissue harvest, joint samples were fixated using 4% paraformaldehyde for 72 hours at 4°C under rotation, followed by paraffin embedding and processing for histological and IHC analysis by cutting tissues into 5-μm-thick tissue sections.

Immunomodulatory cell treatment

aMSC isolation

Subcutaneous abdominal adipose tissue was collected from 15- to 20-week-old male Lewis rats used for other procedures. The adipose tissue was mechanically and enzymatically dissociated [collagenase type IV (100 μg/ml)] to obtain a single aMSC suspension. Cells were seeded in aMSC GM (aGM) consisting of DMEM high-glucose and GlutaMAX-I (Thermo Fisher Scientific, Waltham, MA, USA) supplemented with Humulin R (0.1 U/ml; Lilly USA, Indianapolis, IN), 5% PLTGold Human Platelet Lysate (Biological Industries, Kibbutz Beit HaEmek, Israel), and gentamycin (2.5 μg/ml; Fresenius Kabi, Lake Zurich, IL, USA) for 24 hours. Next, the adhered cells were washed in PBS and cultured at 37°C with 95% O_2 and 5% CO_2 to passage three when they were used for treatment.

MNC isolation

Rat MNCs were obtained from the spleen of 15- to 20-week-old male Lewis rats used for other procedures. Fresh whole rat spleen was obtained under sterile conditions and placed into a petri dish with 5 ml of HBSS (Hank's balanced salt solution) buffer. The spleen was minced into small pieces (~0.2 cm^2) with a scalpel blade. The pieces were then transferred to a 70-μm cell strainer over a 50-ml conical tube. After covering the pieces with HBSS, a plunger was used to wash out the cells from the tissue with repeated addition of HBSS until the tissue turned white. The cells were then centrifuged at 400*g* for 5 min at 4°C, and the supernatant was discarded. Cell pellet was resuspended in red blood cell lysis buffer and incubated for 10 min at room temperature, followed by PBS wash. MNCs were stored in liquid nitrogen until processed for activation.

CAT activation

Isolated MNCs were thawed, washed, and suspended in suspension culture in activation medium consisting of DMEM high glucose and GlutaMAX-I (Thermo Fisher Scientific, Waltham, MA, USA), with the addition of 10% cartilage hydrolysate (Laboratorios Villar, Rosario, Santa Fe, Argentina), famotidine (10 μg/ml; Mylan Institutional LLC, Rockford, IL), indomethacin (4.5 μg/ml; Hospira Inc., Lake Forest, IL, USA), and gentamicin (2.5 μg/ml; Fresenius Kabi, Lake Zurich, IL) at 37°C with 95% O_2 and 5% CO_2.

Coculture

aMSC were cultured in aGM to 70 to 80% confluence and then washed in PBS, and CATs were added in a 4:1 ratio suspended in DMEM high glucose and GlutaMAX-I (Thermo Fisher Scientific, Waltham, MA, USA) supplemented with gentamicin (2.5 μg/ml;

Table 1. Experimental groups.

Experimental condition	Starting age (weeks)	*n*	Days from MIA injection until euthanasia	Start weight (g)	End weight (g)
Controls	8–9	4	7 days	165 (±8.6)	182 (±10.1)
Controls	8–9	6	28 days	178 (±13.9)	218 (±32.3)
Rat ECs	8–9	5 (6)	28 days	165 (±12.2)	206 (±12.8)
Rat aMSCs	8–9	5 (6)	28 days	174 (±5.4)	202 (±1.8)
Rat coculture	8–9	6	28 days	174 (±13.6)	208 (±15.5)

Fresenius Kabi, Lake Zurich, IL, USA). For intra-articular injection, the coculture was maintained for 24 hours at 37°C with 95% O_2 and 5% CO_2. For mechanistic studies, the coculture was maintained for up to 96 hours, followed by mRNA transcript data analysis.

Clinical data

Patients older than 18 years old that consulted the clinic for knee OA (KOA) with a body weight greater than 45 kg and the following blood parameters (hematocrit, ≥35%; mean corpuscular volume ≥ 70%; mean corpuscular hemoglobin ≥ 31%; leukocytes ≥4000/mm^3; and platelets, 150,000 to 400,000/mm^3) with normal cardiac, liver, respiratory, and renal functions were offered the treatment. The inclusion criteria were as follows: Positive KOA diagnosis supported by clinical symptoms and knee abnormalities confirmed by x-ray and or MRI [effusion and synovial thickening/synovitis, subchondral bone marrow edema and/or cysts, cartilaginous defects (partial or full-thickness), bursitis, iliotibial band syndrome]. The pain associated with the MRI characteristics, according to the KOOS scale (*41*), was higher than 80%, and all patients signed the consent form. The exclusion criteria were as follows: Active neoplasm, viral, bacterial, or fungal (internal) active systemic infection at the time of starting the treatment; HIV, hepatitis B, or hepatitis C positive; patients with jaundice or liver failure; pregnant patients; or individuals with alcohol or drug addiction. Ethical considerations were as follows: Documented results are from patients treated with a new investigational drug under compassionate use regulations. All included patients suffered from severe KOA. Their indication was prosthetic replacement of the knee, as OA progression caused a lack of treatment response to standard palliative therapies. The treatment was done under Compassionate Use Conditions. The therapy used is an adaptation of a clinical trial protocol already accepted for evaluation and is registered with the National Administration of Medicines, Food and Technology of Argentina with the file number 1-0047-0002-000209-17-6 presented to treat patients with severe muscular atrophy. The clinical protocol and the text of the Informed Consent Form were approved by the respective IRB of the intervening institutions. Forty eight hours before the start of treatment, patients signed the informed consent form. Patient safety and clinical follow-up were monitored at least once a week to observe treatment safety, efficacy, and effectiveness. Follow-up controls were done approximately 60, 90, 180, and 365 days after treatment, and the latter was mainly used to assess therapeutic effect following the KOOS score and MRI if nothing else stated. This scoring system includes five categories that are self-administered and assessed in a standard questionnaire based on level of (i) pain (9 items assessed), (ii) symptoms (7 items assessed), (iii) activities of daily life (17 items assessed), (iv) sports and recreational activities (5 items assessed), and (v) knee-related quality of life (4 items assessed). Then, a Likert scale is used where all items have five possible answer options scored from zero (no problem) to four (extreme problems). Next, each of the five scores is calculated as the sum of the items included. An aggregate score is not calculated because it is regarded desirable to analyze and interpret the five dimensions separately. The test has previously been evaluated for its test-retest reliability where the intraclass correlation coefficients was regarded as high as previously reported (*41*). The score calculation was then performed and transformed to a 0 to 100 scale where 0 is extreme knee problems and 100 is no knee problem: Transformed scale = 100 − (actual raw score × 100)/(possible raw score range). Statistical evaluation was performed by Wilcoxon nonparametric test to analyze differences before and after treatment. Safety was evaluated according to the National Cancer Institute, USA. The protocol for common terminology criteria for adverse events (version 5.0) was used. MRI of the treated areas was performed approximately 12 months after the end of the treatment test.

Statistical analysis

Descriptive data were expressed as individual data points graphically with or without violin plots representing the data distributions for each outcome. Comparisons between groups were performed using either parametric or nonparametric approaches depending on the outcome being examined. For outcomes measured on either a continuous or an ordinal scale taken on two or more groups, two-way analysis of variance (ANOVA) models with Tukey's post hoc adjustments or Kruskal-Wallis tests were used to compare groups. For analyses where two paired groups were being examined, Wilcoxon signed-rank tests were used. All analyses were performed using Prism (version 9.3; GraphPad Software). Statistical significance was indicated on all graphs as follows between conditions $^*P < 0.05$, $^{**}P < 0.01$, or $^{***}P < 0.001$ unless otherwise stated. Results were conducted from at least three independent experiments ($n = 3$ for in vitro data and $n = 4$ to 6 for in vivo experiments).

Supplementary Materials

This PDF file includes:

Supplementary Materials and Methods
Figs. S1 to S8
Table S1

REFERENCES AND NOTES

1. N. C. Henderson, F. Rieder, T. A. Wynn, Fibrosis: From mechanisms to medicines. *Nature* **587**, 555–566 (2020).
2. H. Long, Q. Liu, H. Yin, K. Wang, N. Diao, Y. Zhang, J. Lin, A. Guo, Prevalence trends of site-specific osteoarthritis from 1990 to 2019: Findings from the global burden of disease study 2019. *Arthritis Rheumatol.* **74**, 1172–1183 (2022).
3. J. Martel-Pelletier, A. J. Barr, F. M. Cicuttini, P. G. Conaghan, C. Cooper, M. B. Goldring, S. R. Goldring, G. Jones, A. J. Teichtahl, J.-P. Pelletier, Osteoarthritis. *Nat. Rev. Dis. Primers* **2**, 16072 (2016).
4. M. Martins-Green, M. Petreaca, L. Wang, Chemokines and their receptors are key players in the orchestra that regulates wound healing. *Adv. Wound Care (New Rochelle)* **2**, 327–347 (2013).
5. N. X. Landen, D. Li, M. Stahle, Transition from inflammation to proliferation: A critical step during wound healing. *Cell. Mol. Life Sci.* **73**, 3861–3885 (2016).
6. S. D. Sommerfeld, C. Cherry, R. M. Schwab, L. Chung, D. R. Maestas Jr., P. Laffont, J. E. Stein, A. Tam, S. Ganguly, F. Housseau, J. M. Taube, D. M. Pardoll, P. Cahan, J. H. Elisseeff, Interleukin-36γ–producing macrophages drive IL-17-mediated fibrosis. *Sci. Immunol.* **4**, eaax4783 (2019).
7. G. Wick, A. Backovic, E. Rabensteiner, N. Plank, C. Schwentner, R. Sgonc, The immunology of fibrosis: Innate and adaptive responses. *Trends Immunol.* **31**, 110–119 (2010).
8. P.-F. Han, L. Wei, Z.-Q. Duan, Z.-L. Zhang, T.-Y. Chen, J.-G. Lu, R.-P. Zhao, X.-M. Cao, P.-C. Li, Z. Lv, X.-C. Wei, Contribution of IL-1β, 6 and TNF-α to the form of post-traumatic osteoarthritis induced by "idealized" anterior cruciate ligament reconstruction in a porcine model. *Int. Immunopharmacol.* **65**, 212–220 (2018).
9. R. S. Decker, H. B. Um, N. A. Dyment, N. Cottingham, Y. Usami, M. Enomoto-Iwamoto, M. S. Kronenberg, P. Maye, D. W. Rowe, E. Koyama, M. Pacifici, Cell origin, volume and arrangement are drivers of articular cartilage formation, morphogenesis and response to injury in mouse limbs. *Dev. Biol.* **426**, 56–68 (2017).
10. E. H. Steen, X. Wang, S. Balaji, M. J. Butte, P. L. Bollyky, S. G. Keswani, The role of the anti-inflammatory cytokine interleukin-10 in tissue fibrosis. *Adv. Wound Care (New Rochelle)* **9**, 184–198 (2020).
11. O. Khoury, A. Atala, S. V. Murphy, Stromal cells from perinatal and adult sources modulate the inflammatory immune response in vitro by decreasing Th1 cell proliferation and cytokine secretion. *Stem Cells Transl. Med.* **9**, 61–73 (2020).
12. W. Liu, Y. Chen, G. Zeng, S. Yang, T. Yang, M. Ma, W. Song, Single-cell profiles of age-related osteoarthritis uncover underlying heterogeneity associated with disease progression. *Front. Mol. Biosci.* **8**, 748360 (2021).
13. H. Nakamura, S. Yoshino, T. Kato, J. Tsuruha, K. Nishioka, T-cell mediated inflammatory pathway in osteoarthritis. *Osteoarthr. Cartil.* **7**, 401–402 (1999).
14. M. K. Haynes, E. L. Hume, J. B. Smith, Phenotypic characterization of inflammatory cells from osteoarthritic synovium and synovial fluids. *Clin. Immunol.* **105**, 315–325 (2002).
15. S. J. Snelling, R. K. Davidson, T. E. Swingler, L. T. T. Le, M. J. Barter, K. L. Culley, A. Price, A. J. Carr, I. M. Clark, Dickkopf-3 is upregulated in osteoarthritis and has a chondroprotective role. *Osteoarthr. Cartil.* **24**, 883–891 (2016).
16. A. Mathiessen, P. G. Conaghan, Synovitis in osteoarthritis: Current understanding with therapeutic implications. *Arthritis Res. Ther.* **19**, 18 (2017).
17. Y. Matsukura, T. Muneta, K. Tsuji, H. Koga, I. Sekiya, Mesenchymal stem cells in synovial fluid increase after meniscus injury. *Clin. Orthop. Relat. Res.* **472**, 1357–1364 (2014).
18. E. M. Roos, L. S. Lohmander, The Knee Injury and Osteoarthritis Outcome Score (KOOS): From joint injury to osteoarthritis. *Health Qual. Life Outcomes* **1**, 64 (2003).
19. E. A. Ross, A. Devitt, J. R. Johnson, Macrophages: The good, the bad, and the gluttony. *Front. Immunol.* **12**, 708186 (2021).
20. T. Morito, T. Muneta, K. Hara, Y. J. Ju, T. Mochizuki, H. Makino, A. Umezawa, I. Sekiya, Synovial fluid-derived mesenchymal stem cells increase after intra-articular ligament injury in humans. *Rheumatology (Oxford)* **47**, 1137–1143 (2008).
21. T. B. Kurth, F. Dell'accio, V. Crouch, A. Augello, P. T. Sharpe, C. De Bari, Functional mesenchymal stem cell niches in adult mouse knee joint synovium in vivo. *Arthritis Rheum.* **63**, 1289–1300 (2011).
22. F. Qu, F. Guilak, R. L. Mauck, Cell migration: implications for repair and regeneration in joint disease. *Nat. Rev. Rheumatol.* **15**, 167–179 (2019).
23. A. Gomez-Aristizabal, R. Gandhi, N. N. Mahomed, K. W. Marshall, S. Viswanathan, Synovial fluid monocyte/macrophage subsets and their correlation to patient-reported outcomes in osteoarthritic patients: A cohort study. *Arthritis Res. Ther.* **21**, 26 (2019).
24. M. Mellado, L. Martinez-Munoz, G. Cascio, P. Lucas, J. L. Pablos, J. M. Rodriguez-Frade, T cell migration in rheumatoid arthritis. *Front. Immunol.* **6**, 384 (2015).
25. D. Mulherin, O. Fitzgerald, B. Bresnihan, Synovial tissue macrophage populations and articular damage in rheumatoid arthritis. *Arthritis Rheum.* **39**, 115–124 (1996).
26. P. P. Tak, T. J. Smeets, M. R. Daha, P. M. Kluin, K. A. Meijers, R. Brand, A. E. Meinders, F. C. Breedveld, Analysis of the synovial cell infiltrate in early rheumatoid synovial tissue in relation to local disease activity. *Arthritis Rheum.* **40**, 217–225 (1997).
27. T. Sono, C.-Y. Hsu, Y. Wang, J. Xu, M. Cherief, S. Marini, A. K. Huber, S. Miller, B. Peault, B. Levi, A. W. James, Perivascular fibro-adipogenic progenitor tracing during post-traumatic osteoarthritis. *Am. J. Pathol.* **190**, 1909–1920 (2020).
28. L. Wu, F. A. Petrigliano, K. Ba, S. Lee, J. Bogdanov, D. R. McAllister, J. S. Adams, A. K. Rosenthal, B. Van Handel, G. M. Crooks, Y. Lin, D. Evseenko, Lysophosphatidic acid mediates fibrosis in injured joints by regulating collagen type I biosynthesis. *Osteoarthr. Cartil.* **23**, 308–318 (2015).
29. J. Bolander, W. Ji, J. Leijten, L. M. Teixeira, V. Bloemen, D. Lambrechts, M. Chaklader, F. P. Luyten, Healing of a large long-bone defect through serum-free in vitro priming of human periosteum-derived cells. *Stem Cell Rep.* **8**, 758–772 (2017).
30. C.-W. Huang, W.-C. Huang, X. Qiu, F. F. F. da Silva, A. Wang, S. Patel, L. J. Nesti, M.-M. Poo, S. Li, The differentiation stage of transplanted stem cells modulates nerve regeneration. *Sci. Rep.* **7**, 17401 (2017).
31. G. A. Moviglia, M. T. M. Brandolino, D. Couto, S. Piccone, Local immunomodulation and muscle progenitor cells induce recovery in atrophied muscles in spinal cord injury patients. *J. Neurorestoratology* **6**, 136–145 (2018).
32. J. Li, J. Tan, M. M. Martino, K. O. Lui, Regulatory T-cells: Potential regulator of tissue repair and regeneration. *Front. Immunol.* **9**, 585 (2018).
33. A. C. Poholek, Tissue-specific contributions to control of T cell immunity. *Immunohorizons* **5**, 410–423 (2021).
34. T. Sakamoto, T. Miyazaki, S. Watanabe, A. Takahashi, K. Honjoh, H. Nakajima, H. Oki, Y. Kokubo, A. Matsumine, Intraarticular injection of processed lipoaspirate cells has anti-inflammatory and analgesic effects but does not improve degenerative changes in murine monoiodoacetate-induced osteoarthritis. *BMC Musculoskelet. Disord.* **20**, 335 (2019).
35. L. Mei, B. Shen, P. Ling, S. Liu, J. Xue, F. Liu, H. Shao, J. Chen, A. Ma, X. Liu, Culture-expanded allogenic adipose tissue-derived stem cells attenuate cartilage degeneration in an experimental rat osteoarthritis model. *PLOS ONE* **12**, e0176107 (2017).
36. R. F. Schelbergen, S. van Dalen, M. ter Huurne, J. Roth, T. Vogl, D. Noel, C. Jorgensen, W. B. van den Berg, F. A. van de Loo, A. B. Blom, P. L. van Lent, Treatment efficacy of adipose-derived stem cells in experimental osteoarthritis is driven by high synovial activation and reflected by S100A8/A9 serum levels. *Osteoarthr. Cartil.* **22**, 1158–1166 (2014).
37. E. T. Hurley, Y. Yasui, A. L. Gianakos, D. Seow, Y. Shimozono, G. Kerkhoffs, J. G. Kennedy, Limited evidence for adipose-derived stem cell therapy on the treatment of osteoarthritis. *Knee Surg. Sports Traumatol. Arthrosc.* **26**, 3499–3507 (2018).
38. K. P. H. Pritzker, S. Gay, S. A. Jimenez, K. Ostergaard, J.-P. Pelletier, P. A. Revell, D. Salter, W. B. van den Berg, Osteoarthritis cartilage histopathology: Grading and staging. *Osteoarthr. Cartil.* **14**, 13–29 (2006).
39. C. Guingamp, P. Gegout-Pottie, L. Philippe, B. Terlain, P. Netter, P. Gillet, Mono-iodoacetate-induced experimental osteoarthritis: A dose-response study of loss of mobility, morphology, and biochemistry. *Arthritis Rheum.* **40**, 1670–1679 (1997).
40. M. Udo, T. Muneta, K. Tsuji, N. Ozeki, Y. Nakagawa, T. Ohara, R. Saito, K. Yanagisawa, H. Koga, I. Sekiya, Monoiodoacetic acid induces arthritis and synovitis in rats in a dose- and time-dependent manner:Pproposed model-specific scoring systems. *Osteoarthr. Cartil.* **24**, 1284–1291 (2016).
41. E. M. Roos, H. P. Roos, L. S. Lohmander, C. Ekdahl, B. D. Beynnon, Knee Injury and Osteoarthritis Outcome Score (KOOS)—Development of a self-administered outcome measure. *J. Orthop. Sports Phys. Ther.* **28**, 88–96 (1998).

Acknowledgments

Funding: The research was funded partly by the Research Foundation - Flanders through research grant 1518618N, the postdoctoral grant 12S6817N, and the B.A.E.F. Henri Benedictus Fellowship. **Author contributions:** J.B., G.M., and A.A. conceived and designed the study. J.B. and E.P. performed in vitro experiments and generated data. J.B., W.V., and G.M. performed in vivo experiments. J.B. and O.J. performed analysis from in vivo experiments. G.P. collected clinical SF samples and evaluated MRIs. M.T.M.B. managed clinical data. J.B. wrote the manuscript. O.J., W.V., G.M., E.P., and A.A. edited the manuscript. All authors read and approved the final draft of the manuscript. **Competing interests:** The authors declare that they have no competing interests. A patent has been filed for the described cell therapy no. 63/279,316, Wake Forest University Health Sciences, with inventors: J.B., G.M., and A.A., 15 November 2021. **Data and materials availability:** All data needed to evaluate the conclusions in the paper are present in the paper and/or the Supplementary Materials.

Submitted 17 August 2022
Accepted 16 March 2023
Published 21 April 2023
10.1126/sciadv.ade4645

ScienceAdvances

The synovial environment steers cartilage deterioration and regeneration

Johanna Bolander, Maria Teresita Moviglia Brandolina, Gary Poehling, Olivia Jochl, Emma Parsons, William Vaughan, Gustavo Moviglia, and Anthony Atala

Sci. Adv., **9** (16), eade4645.
DOI: 10.1126/sciadv.ade4645